

# Implantable and Biodegradable Poly(L-lactic acid) Fibers for Optical Neural Interfaces

Ruxing Fu, Wenhan Luo, Roya Nazempour, Daxin Tan, He Ding, Kaiyuan Zhang, Lan Yin, Jisong Guan,\* and Xing Sheng\*

Advanced optical fibers and photonic structures play important roles in neuroscience research, along with recent progresses of genetically encoded optical actuators and indicators. Most techniques for optical neural implants rely on fused silica or long-lasting polymeric fiber structures. In this paper, implantable and biodegradable optical fibers based on poly(L-lactic acid) (PLLA) are presented. PLLA fibers with dimensions similar to standard silica fibers are constructed using a simple thermal drawing process at around 220 °C. The formed PLLA fibers exhibit high mechanical flexibility and optical transparency, and their structural evolution and optical property changes are systematically studied during in vitro degradation. In addition, their biocompatibility with brain tissues is evaluated in living mice, and full in vivo degradation is demonstrated. Finally, PLLA fibers are implemented as a tool for intracranial light delivery and detection, realizing deep brain fluorescence sensing and optogenetic interrogation in vivo. The presented materials and device platform offer paths to fully biocompatible and bioresorbable photonic systems for biomedical uses.

represent inferior compatibility with biological systems (especially soft brain tissues) due to their high stiffness and long-time stability, which lead to deleterious effects like tissue damage, inflammation, and rejection.<sup>[4]</sup> Flexible and stretchable polymeric fibers with designed microstructures are explored for neurological studies, enabling integrated electrical sensing, optical stimulation, and controlled microfluidic delivery.<sup>[5]</sup> In medical practice, biodegradable organic and inorganic materials including metals, semiconductors, and polymers have been exploited to form biological structures (drugs, stents, scaffolds, etc.)<sup>[6]</sup> and functional devices (electrical, optical, mechanical, and thermal sensors).<sup>[7]</sup> In comparison to devices and systems made of inert materials, these biodegradable implants that can physically disappear in biological tissues to eliminate the risk

## 1. Introduction


Implantable optical waveguides deliver optical signals and energy into deep tissues, enabling important applications in biomedical fields including optogenetic stimulation,<sup>[1]</sup> fluorescence photometry,<sup>[2]</sup> laser surgery, and phototherapy.<sup>[3]</sup> Conventional silica-based fibers serve as standard tools for optical implants,<sup>[1,2]</sup> holding advantages like mature fabrication methods, low loss, and high stability. However, silica fibers

associated with further retraction or removal, providing enormous potential to biomedical applications and particularly clinical uses. Recently, waveguides and photonic structures based on biodegradable materials like ceramics (e.g., calcium phosphates),<sup>[8]</sup> synthetic polymers,<sup>[9]</sup> hydrogels,<sup>[10]</sup> and even bioderived materials (e.g., silks)<sup>[11]</sup> are investigated in both in vitro and in vivo studies. So far, these biodegradable photonic materials and structures have not been utilized as implantable fibers to study deep-brain neural activities. Here, we present poly(L-lactic acid) (PLLA)-based optical fibers as a biodegradable

R. Fu, R. Nazempour, Dr. H. Ding, K. Zhang, Prof. X. Sheng  
Department of Electronic Engineering  
Tsinghua National Laboratory for Information Science  
and Technology (TNList)  
Tsinghua University  
Beijing 100084, China  
E-mail: xingsheng@tsinghua.edu.cn

R. Fu, D. Tan, K. Zhang, Prof. L. Yin  
School of Materials Science and Engineering  
Tsinghua University  
Beijing 100084, China

W. Luo  
Peking-Tsinghua Center for Life Sciences  
Beijing 100871, China

 The ORCID identification number(s) for the author(s) of this article can be found under <https://doi.org/10.1002/adom.201700941>.

W. Luo  
Academy for Advanced Interdisciplinary Studies  
Peking University  
Beijing 100871, China  
W. Luo, Prof. J. Guan  
MOE Key Laboratory of Protein Sciences  
Center for Brain inspired Computing  
IDG/McGovern institute for Brain Research at Tsinghua  
School of Life Sciences  
Tsinghua University  
Beijing 100084, China  
Prof. J. Guan  
School of Life Science and Technology  
ShanghaiTech University  
Shanghai 201210, China  
E-mail: guanjs@shanghaitech.edu.cn

DOI: 10.1002/adom.201700941

optical neural interface. The PLLA fibers are formed via thermal drawing process and their optical, structural, mechanical, and thermal properties are systematically investigated. Degradation behaviors of fibers during *in vitro* hydrolysis are studied, and their optical properties are experimentally measured and numerically simulated. Furthermore, the fibers are injected deeply into brains of living mice, with demonstrated natural dissolution in neural systems. Finally, *in vivo* neural activity studies including fluorescence signal collection and optogenetic stimulation illustrate their capabilities for use in freely moving animals. These results provide viable routes for fully degradable optics/biology interfaces with versatile biomedical applications.

## 2. Fiber Fabrication and Characterizations

PLLA-based optical fibers are fabricated by the thermal drawing process, schematically illustrated in Figure 1A. The PLLA polymer crystalline powders are melted at about 220 °C and drawn as fibers, and then the soft polymer fibers are cooled down along with a crystalline-to-amorphous phase transition. Fiber diameters are controlled by modifying the drawing speed, and fibers with a diameter of about 220  $\mu\text{m}$  are used throughout the paper to connect with standard optical measurement setups for biological research. The scanning electron microscopy (SEM) image in Figure 1B illustrates the fiber geometry. The cylindrical fiber structure serves as a waveguide with guided photons

undergoing total internal reflection at interfaces between the PLLA polymer (refractive index  $n = 1.47$  and transparent in the visible ranges)<sup>[12]</sup> and outer media, such as air ( $n = 1.0$ ), dermal tissues ( $n = 1.38\text{--}1.44$ ),<sup>[13]</sup> and brain tissues ( $n = 1.36\text{--}1.42$ ).<sup>[14]</sup> To simplify the process, no cladding layer is applied outside the PLLA fiber, while transparent biodegradable organic materials with a lower refractive index (for example, alginate hydrogels with  $n = 1.34$ )<sup>[10b]</sup> can be employed as cladding for further optical loss reduction (see Figure S1 in the Supporting Information). The 220  $\mu\text{m}$  diameter fibers can be coupled with ceramic ferrules and linked to external laser and/or light-emitting diode (LED)-based light sources as shown in Figure 1C. With a measured bending stiffness of  $\approx 1.5 \times 10^4 \text{ N m}^{-1}$ , the PLLA fibers exhibit higher flexibility and therefore better biocompatibility than conventional fused silica fibers with the same geometries (stiffness of  $2.4 \times 10^5 \text{ N m}^{-1}$ ) (see Figure S2 in the Supporting Information). These measurements are in agreement with calculated results based on Young's moduli of these materials.<sup>[5a,6a]</sup> Similar drawing approaches can be exploited at a slightly lower heating temperature ( $\approx 200^\circ\text{C}$ ) to fabricate poly(lactic-co-glycolic acid) (PLGA)-based fibers with different ratios of lactic and glycolic acids, such as PLGA 75:25 (with lactide:glycolide = 75:25), PLGA 50:50, and PLGA 65:35. These PLGA and PLLA fibers exhibit similar mechanical properties around 37 °C, with measurement results in Figure S2B (Supporting Information) as an example.

X-ray diffraction (XRD) and differential scanning calorimetry (DSC) (Figure 1D,E, respectively) measure structures and

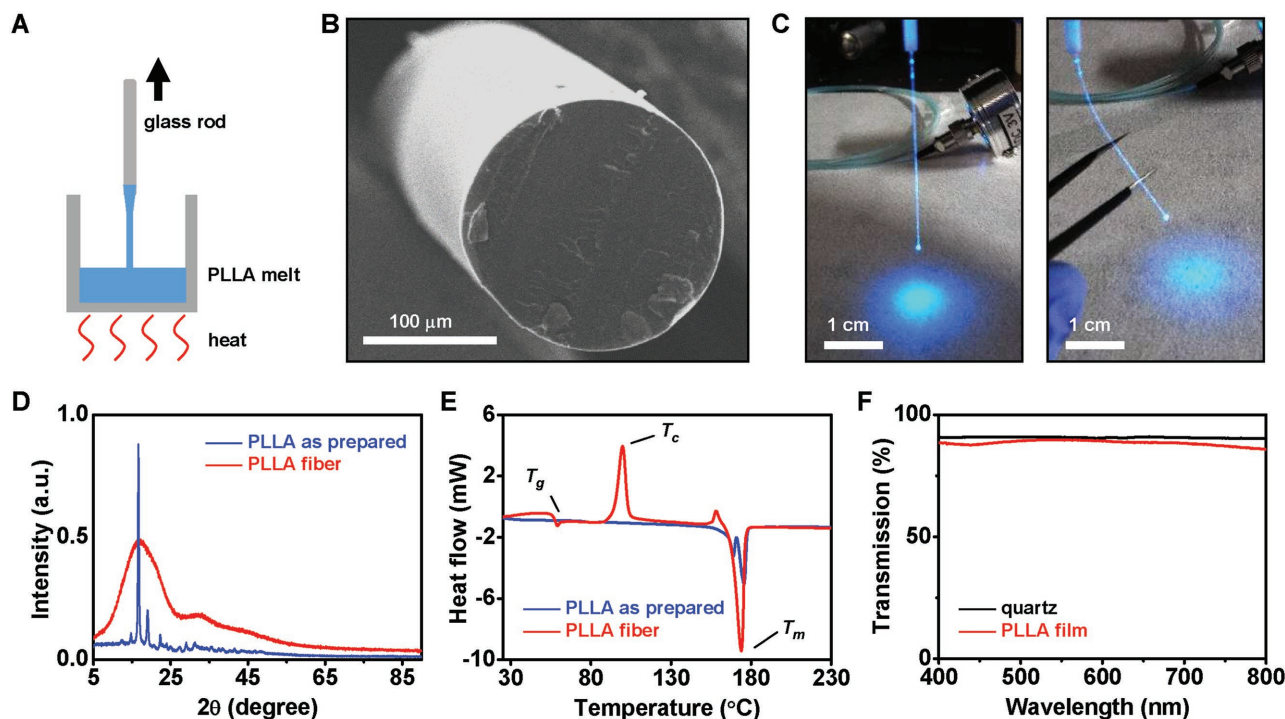


**Figure 1.** Fabrication and characterization of biodegradable PLLA fibers. A) Schematic illustration of the thermal drawing process. B) SEM image (cross-sectional view) of the PLLA fiber with a diameter of about 220  $\mu\text{m}$ . C) A 5 cm long PLLA fiber coupled to a blue LED (473 nm). Left, no bending; right, bended with a tweezer. D) XRD patterns of as-prepared PLLA powders and drawn PLLA fibers. E) DSC results of as-prepared PLLA powders and drawn PLLA fibers, showing a glass transition temperature  $T_g = 65^\circ\text{C}$ , a crystallization temperature  $T_c = 100^\circ\text{C}$ , and a melting temperature  $T_m = 175^\circ\text{C}$ . F) Optical transmission spectra of quartz substrates with and without a coated PLLA film (thickness:  $\approx 10 \mu\text{m}$ ).

thermal properties of as-prepared PLLA powders and thermally drawn PLLA fibers. Figure 1D shows the XRD patterns of PLLA as-prepared and the fiber, in which as-prepared PLLA shows diffraction peaks at  $2\theta = 17^\circ$  and  $19^\circ$ . The diffraction spectrum of thermally drawn PLLA fibers exhibits a much broader peak, which reveals the crystalline-to-amorphous transition.<sup>[15]</sup> DSC results indicate that the amorphous PLLA fiber exhibits a glass transition temperature  $T_g$  at  $65^\circ\text{C}$  and a crystallization temperature  $T_c$  at  $100^\circ\text{C}$ , while the as-prepared crystalline PLLA powders do not reveal apparent glass transition and crystallization. Both PLLA fibers and as-prepared powders melt at  $T_m = 175^\circ\text{C}$ . Measured optical transmission spectra (Figure 1F) show that the amorphous state PLLA films have similar optical transparency with quartz glasses. The negligible intrinsic optical losses in the visible range agree with the measured transmission ( $\approx 95\%$  in the visible range) of PLLA in literature.<sup>[12b,16]</sup> The structural, mechanical, thermal, and optical properties of PLLA fibers along with its manufacturability make it a viable solution to implantable waveguides for biomedical applications.

### 3. Evolution of Optical Properties with Biodegradation In Vitro

PLLA- and PLGA-based polymers act as widely used structural materials for biomedical implants.<sup>[6]</sup> By tuning ratios of lactic/glycolic acids and polymer molecular weights, PLLA/PLGA degradation periods span from weeks to years.<sup>[17]</sup> While their hydrolytic degradation processes have been extensively studied,<sup>[18]</sup> there are very few studies that have looked into the evolution of optical properties along with biodegradation.<sup>[9]</sup> Figures 2 and 3

characterize the structural evolution and associated optical property changes of PLLA-based thin films and optical fibers in vitro. PLLA films coated on glass substrates are immersed into phosphate buffer solutions (PBS) with  $\text{pH} = 7.4$  at  $37^\circ\text{C}$ . Atomic force microscopic (AFM) images in Figure 2A present surface morphologies of PLLA films soaked in the PBS for 0–42 d, with measured mean roughness (Ra) shown in Figure 2B. Consistent with the SEM image in Figure 1B, the as-prepared PLLA (day-0) is very smooth with  $R_a = 0.29\text{ nm}$ , resulting in very low scattering for the fiber waveguides. During hydrolysis, ester bonds in polymer chains react with the water, break up, and form smaller chains that dissolve into the water, generating surface defects.<sup>[17]</sup> From day-0 to day-7, both the size and density of surface defects increase with time, resulting in an increased Ra. Results from day-7 to day-28 probably indicate that surface erosion has reached a steady state and bulk erosion start to dominate. After 28 d in PBS, severe bulk erosion<sup>[17]</sup> occurs and the PLLA surface becomes very rough with  $R_a > 9.5\text{ nm}$ .

To further investigate the influence of surface morphology on optical properties of PLLA fibers during biodegradation, thermally drawn PLLA fibers are immersed into PBS. Microscopic optical images in Figure 2C illustrate a PLLA fiber before and after immersion in PBS (day-24). The surface erosion of PLLA fibers is consistent with the aforementioned results obtained in PLLA films. The eroded surface generates scatterings and thereby causes increased propagation losses in fibers. This is illustrated in vitro by embedding the PLLA fibers into hydrogel-based brain phantoms. Figure 2D compares light propagation ( $473\text{ nm}$ ) behaviors of a PLLA fiber injected in slices of brain phantoms before (left) and after (right) immersion in PBS (day-7). Although the as-prepared PLLA fiber has

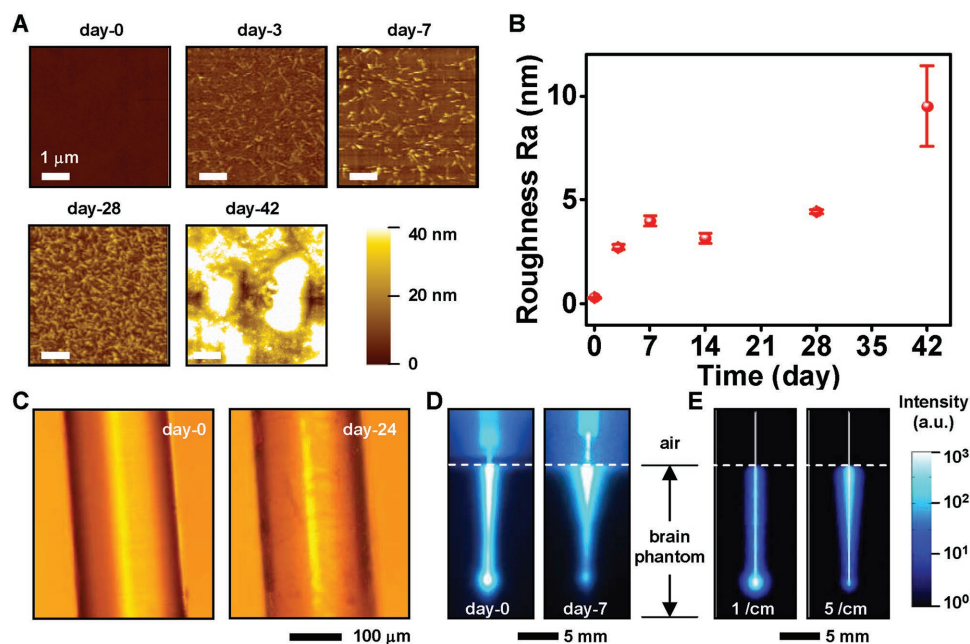


**Figure 2.** Characterization of surface morphology for PLLA films and fibers degraded in vitro. A) AFM images of PLLA films soaked in PBS for various days. B) Measured mean surface roughness ( $R_a$ ) of PLLA films as a function of soaked time. C) Optical images of a PLLA fiber before (left) and after (right) being soaked in PBS for 24 d. D) Optical images of a PLLA fiber guiding light ( $473\text{ nm}$ ) in brain phantom before (left) and after (right) being soaked in PBS for 7 d. E) Simulated optical power distribution of PLLA fibers guiding light ( $473\text{ nm}$ ) in brain phantom, with fiber scattering coefficients of  $1.0\text{ cm}^{-1}$  (left) and  $5.0\text{ cm}^{-1}$  (right).

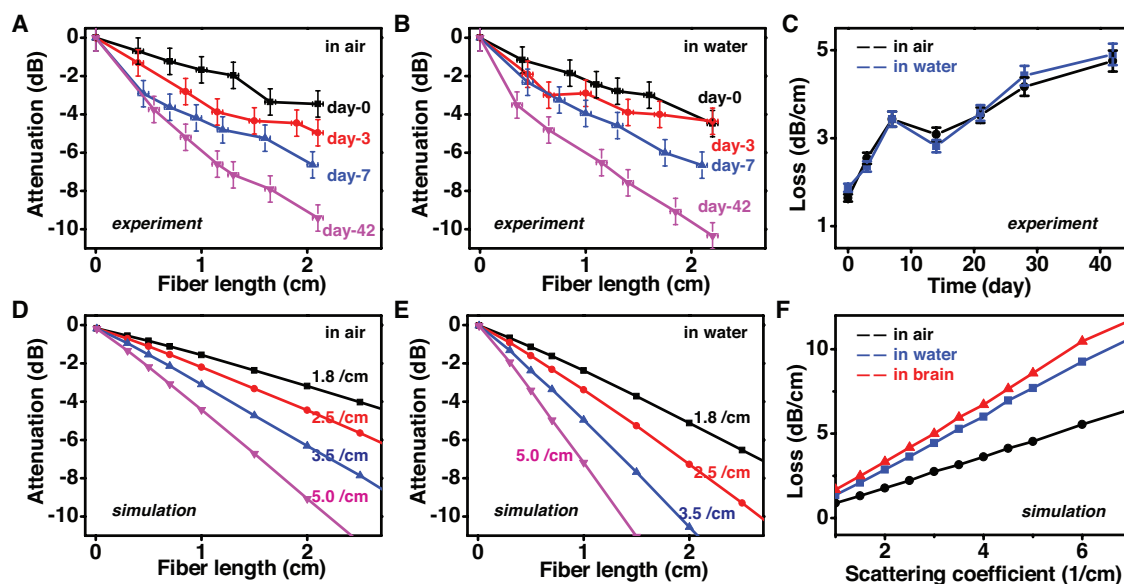


**Figure 3.** Measured and simulated optical properties for PLLA fibers degraded in vitro. A) Normalized optical attenuation for PLLA fibers soaked in PBS for different times at the wavelength of 473 nm, measured in the air. B) Normalized optical attenuation for the same fibers as in (A) measured in water. C) Measured propagation loss of PLLA fibers as a function of soaking time. D) Simulated optical attenuation in the air for PLLA fibers with different scattering coefficients (1.8, 2.5, 3.5, and 5.0  $\text{cm}^{-1}$ ). E) Simulated optical attenuation in water for the same fibers as in (D). F) Calculated propagation loss of PLLA fibers in air, water, and brain tissues, as a function of scattering coefficients.

a smooth surface, optical leakage can still be observed at the fiber/phantom interface, because of the intrinsic scattering in the brain phantom. After degradation (right), increased surface roughness generates stronger scatterings and a considerable propagation loss can be observed within the injection depth of less than 4 mm, with less light transmitted to the fiber end (at a depth of 15 mm). Figure 2E illustrates ray-tracing simulation results consistent with experiments in Figure 2D, by modeling fibers with different scattering coefficients (left: 1.0  $\text{cm}^{-1}$ , right: 5.0  $\text{cm}^{-1}$ ).

To quantitatively evaluate the change of fiber optical properties associated with hydrolysis, we numerically and experimentally investigate the optical transmittance and propagation loss of PLLA fibers in different media (air, water, and tissue) after being soaked in PBS for various periods of time. Figure 3A,B presents measured transmittance of fibers with different lengths in the air and water, respectively. A 473 nm blue LED serves as the light source and connect to the fiber via a standard ceramic ferrule, and transmitted light power is collected with a standard silicon photodiode. Fiber lengths are adjusted by a cutback technique.<sup>[19]</sup> Measured fiber loss coefficients in the air and water are plotted in Figure 3C. Loss coefficients for as-prepared (day-0) PLLA fibers are 1.64  $\text{dB cm}^{-1}$  in the air and 1.87  $\text{dB cm}^{-1}$  in water. Loss coefficients increase with time and reach 4.75 and 4.90  $\text{dB cm}^{-1}$  in the air and water, respectively. The increased propagation loss is mainly attributed to the scattering induced by increased surface roughness as reported in Figure 2. In comparison, Figure 3D–F plots calculated fiber transmittance and propagation losses by ray tracing simulations. In Figure 3D,E, different scattering coefficients (1.8, 2.5, 3.5, and 5.0  $\text{cm}^{-1}$ ) in fibers are incorporated into the models to calculate the fiber transmittance in the air and water at different lengths. While calculated fiber losses in water are higher

than those in the air, measured results in the two media are very similar. This is likely due to the uncertainties in putting photodiodes to measure the optical output power in the water. Although it is difficult to design experiments to measure fiber propagation losses in real brain tissues, numerical models can be established to predict the fiber performance in the brain, with results also included in Figure 3F. Despite the fact that biological tissues usually exhibit much stronger absorption and scattering than pure water, simulated results indicate that PLLA fibers embedded in brain tissues only present slightly higher losses than the same fibers in water. This is because the refractive index of brain tissues ( $n = 1.36$ ) is very close to that of water ( $n = 1.33$ ). Therefore, the total internal reflection condition at the PLLA/brain interface still holds for most of the photons in the waveguide.

#### 4. In Vivo Evaluation of Biocompatibility and Biodegradability

The biocompatibility of implantable and degradable polymer fibers is evaluated and in vivo results are shown in Figure 4. In vitro results presented in Figures 2 and 3 reveal structural and optical property evolutions of PLLA fibers soaked in PBS for up to 42 d. Based on previous reports,<sup>[17]</sup> fully degradation of PLLA in biological systems could take one to two years. To demonstrate the concepts, here we carry out accelerated experiments in vivo by using fibers made from PLGA 50:50 (with lactide:glycolide = 50:50) with a shorter degradation time.<sup>[10]</sup> The PLGA 50:50 fiber used here has a similar molecular weight and mechanical/thermal properties to the previously used PLLA, and can be fabricated by the same drawing approach. PLGA fibers are implanted into brains of multiple



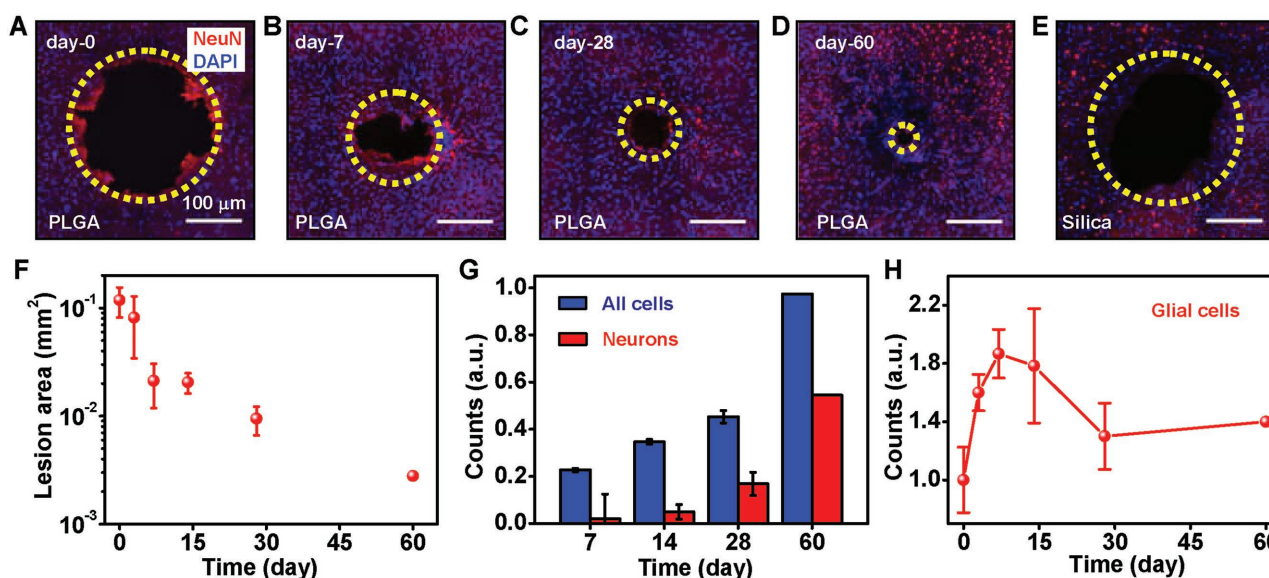


**Figure 4.** In vivo biocompatibility and biodegradation tests of PLGA fibers. A–D) Confocal fluorescence images of horizontal brain slices of mice after fiber implantation for various days. Areas of lesion caused after implantation of PLGA fibers decreases and the cells recover as shown by immunohistochemically staining of neurons (NeuN: a biomarker for neurons, red) and all the cells (DAPI: 4',6-diamidino-2-phenylindole, blue). E) Confocal fluorescence image of horizontal brain slices after implantation of the silica fiber. F) Measured lesion areas as a function of injection time. G) Counts of glial cells near the lesion area (circle, diameter 250  $\mu\text{m}$ ). The results are normalized to that in the normal tissue. H) Recovery of cells in the area of implantation. The data are normalized to the intact tissue away from the lesion part (diameter of 220  $\mu\text{m}$ ).

three month old mice at a depth of 2.5 mm (cover the whole depth of cortex), with perfusion and brain section performed after different days (Figure 4A–F). On the day of implantation (day-0) (Figure 4A), the area of the lesion created by the PLGA fiber is almost equivalent to that of a silica fiber with similar geometries (Figure 4F). PLGA fibers fully dissolve in the mouse brain about two weeks after the implantation, which is proved by retracting the implants. Along with the PLGA fiber dissolution, lesion in the brain region is gradually reduced and almost disappears on day-60 (Figure 4E). By contrast, retracting PLGA and PLLA fibers directly from the brain tissue before their degradation sometimes takes away living tissues and creates severe damage, exemplified in Figure S3 (Supporting Information). Effects of lesion are quantified and plotted in Figure 4G,H. Along with reduced lesion areas, significant recoveries occur for neurons (NeuN) and all the cells (DAPI) in lesion regions. It can be observed that the cell number keeps increasing after the implantation and recovers to the number as intact tissues (away from lesion), and the number of neurons also recover to about 50% of normal condition. The recovery mechanism can be explained by that glial cells are recruited to the injured site to fill the tissue gap and help neurons regenerate in the site. Meanwhile, the inflammation is evaluated by comparing glial cells near the lesion area to normal condition, shown in Figure 4H. The number of glial cells acutely increases at the first week, and then slowly decreases and recovers to a level close to the normal condition from day-28, which indicates that inflammation subsides gradually.<sup>[20]</sup> These results demonstrate desirable biodegradability and biocompatibility of the thermal-drawn PLGA and PLLA fibers, which can be further utilized for neural activity studies.

## 5. In Vivo Neural Signal Sensing and Interrogation

In this part, PLLA fibers are applied for in vivo brain function tests including neural signal sensing and interrogation, and their light guiding performances are evaluated during biodegradation (Figure 5). PLLA fibers are implanted into brains of freely moving mice and linked to standard optical setups (ferrules, fibers, filters, lasers, detectors, etc.) for photometric and optogenetic experiments (Figure 5A,B).<sup>[1,3]</sup> For proof-of-concept demonstration, deep brain fluorescence recording is performed in hypothalamus (HY). The HY of mice is injected with the AAV-CMV-EGFP virus, which indiscriminately infects all kinds of cells and leads to a high expression of enhanced green fluorescence protein (EGFP) (Figure 5C).<sup>[21]</sup> After two weeks of full EGFP expression, 5.5 mm long PLLA fibers are implanted in right hemisphere. Meanwhile, standard silica fibers are injected in left hemisphere as reference to eliminate systematic errors from the measurement setup. The excitation light (488 nm) from a laser source is delivered via the fiber into the HY and the green fluorescence from EGFP is collected and guided by the same fiber and then received by a standard detector. Figure 5D plots the collected fluorescence intensity in vivo from PLLA fibers (normalized to signals from silica fibers) at various days after implantation. Results indicate that the intensity of received fluorescence from PLLA fibers decreases along with time compared to silica fibers. This is consistent with the in vitro measurements and simulated results mentioned above.

Optogenetic experiments with PLLA fibers are performed and results are presented in Figure 5E–G. One classic stimulation manipulation with obvious phenotypes is hyperactivating hippocampus (HPC) neurons to induce seizures, which arouse abnormal behaviors of mice with enhanced locomotion compared to the normal condition.<sup>[22]</sup> The AAV-DIO-oChIEF-mCherry

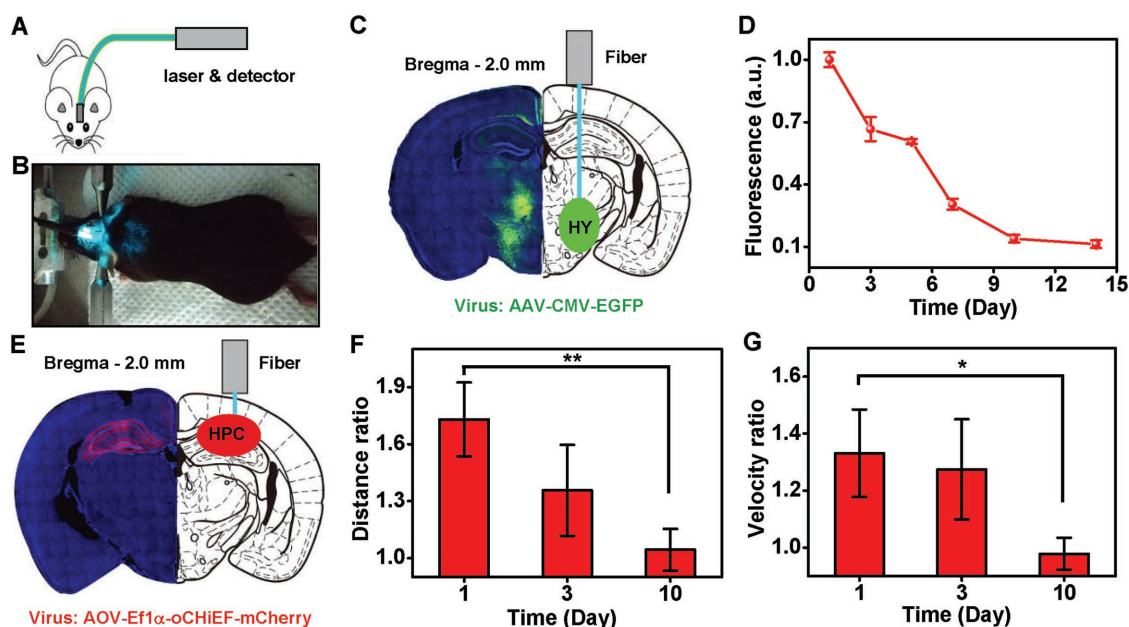


**Figure 5.** In vivo fluorescence photometry and optogenetic experiments with PLLA fibers. A) Schematic cartoon of the experiment design. B) Photographic image of a mouse implanted with a PLLA fiber connected to an external laser (488 nm). C) Left: confocal microscopic image of a coronal section containing EGFP two weeks after viral transfection. Right: schematic illustration of the fiber implanted into the HY. D) Measured fluorescence signals recorded via PLLA fibers (standard deviation,  $n = 6$ ) normalized to those measured via silica fibers. The decrease with time reveals the degradation of PLLA fibers in vivo. E) Left: confocal microscopic image of a coronal section containing oChIEF protein two weeks after viral transfection. Right: schematic illustration of the fiber implanted into the HPC. F) Ratio of travelling distance with the laser on and off (one-tailed  $t$ -test,  $**p < 0.01$ , standard error of mean,  $n = 6$ ). G) Ratio of travelling velocity with the laser on and off (one-tailed  $t$ -test,  $*p < 0.05$ , standard error of mean,  $n = 6$ ).

virus that specifically infects excitatory neurons is injected into the bilateral HPC of CamkII-cre mice (Figure 5E). After two week fully expression of the oChIEF protein,<sup>[23]</sup> PLLA fibers are implanted and optical stimulation signals are applied with a 473 nm laser. Figure 5F,G summarizes measured distance and velocity ratios of mice travelling with and without optical stimulations. When the laser is applied on day-1, light is guided to the HPC via PLLA fibers, inducing a mild seizure that excites the mice with increased travelling distances and velocities (Movie S1, Supporting Information). When the laser is turned off, mice immediately recover to their normal states. Similar experiments are repeated on day-3 and day-10, in which the same incident laser power is applied. Both distance and velocity ratios significantly decrease with time and eventually mice act as normal no matter when the laser turned on or off on day-10 (Movie S2, Supporting Information). In contrast, seizures can still be induced on day-10 in the same mice with silica fibers implanted on the other side of brains. Even though PLLA fibers cannot be fully dissolved within 10–15 d, in vivo results clearly indicate their performance degradation and capability changes for neural activity research.

## 6. Conclusion

With the development of optical technologies for biomedical applications, implantable optical waveguides and fibers are explored to deliver light into tissues for sensing or phototherapy.<sup>[10]</sup> Biocompatible, especially biodegradable implantable devices have become an important research direction in biomedical fields considering potential clinical uses. The results

presented in this paper clearly demonstrate that thermally drawn PLLA fibers as well as related materials and devices provide routes to advanced biodegradable optical neural interfaces. PLLA- and general PLGA-based polymers, which have been widely used as biodegradable polymers in tissue engineering, exhibit desirable features to serve as biodegradable optical fibers, including the ease of fabrication, controllable degradation rates, ideal flexibility, and optical transparency. It is envisioned that standard fiber drawing towers or extrusion-molding methods<sup>[24]</sup> would be used for continuous and massive fiber fabrication. In our current work, lack of cladding causes additional leakage of light throughout the fibers, especially when they are embedded into the tissue with high optical scattering and absorption. Future directions include the development of step-index or graded-index fiber structures<sup>[10b]</sup> made by multi-layered fully degradable materials (hydrogels, polymers, etc.) for improved optical performance and operation stability, with preliminary results shown in Figure S1 (Supporting Information). In addition, optically or thermally triggered biodegradable materials<sup>[25]</sup> can be applied as cladding or core materials in fibers, which maintain their optical properties during in vivo operation and provide a rapid and controllable degradation after use. Considering diverse and multifunctional demands in biomedical fields, advanced fiber architectures can be designed and fabricated by combining conductive wires for electrical recording<sup>[26]</sup> and hollow channels for drug delivery.<sup>[5]</sup> Besides fluorescence photometry and optogenetic stimulation, other applications including laser surgery<sup>[3]</sup> and phototherapy<sup>[9]</sup> can also be exploited. Biodegradable fibers and waveguides can also be integrated with physically transient semiconductor-based

sensors.<sup>[7]</sup> To summarize, results presented here suggest promising pathways toward fully biodegradable photonic devices and systems for fundamental biological studies and even clinical uses within the human body.

## 7. Experimental Section

**Fabrication of Biodegradable Fibers:** PLLA ( $M_w = 55\,000$  Da) and PLGA ( $M_w = 70\,000$  Da, lactic to glycolic monomer ratio of 50:50) (Jinan Daigang Biomaterial Co., Ltd.) were purchased as dry powders. The powders in a beaker were heated to about 220 °C on a hot plate and melt. Subsequently, PLLA and PLGA fibers could be thermally drawn from the melt with glass capillary tubes. Diameters of fibers were controlled by adjusting the drawing speed. To accommodate with standard ceramic (Zirconia) ferrules connected with optical measurement setups, cylindrical fibers with a diameter of about 220  $\mu\text{m}$  were used throughout the paper. Standard fused silica fibers (200  $\mu\text{m}$  core diameter, 220  $\mu\text{m}$  cladding diameter, numerical aperture = 0.37, Newdoon Inc.) were also used in some *in vivo* experiments. PLLA thin films were formed by blade coating of the melt for optical transmission and surface roughness measurements.

**Characterization:** XRD measurements were carried out by SmartLab Diffractometer (Rigaku). DSC measurements were performed by DSC Q2000 (TA Instruments) scanning from 20 to 300 °C, with a ramping rate of 10 °C  $\text{min}^{-1}$ . The DSC and XRD characterize the properties of both PLLA powders and fibers. The SEM images were collected by ZEISS Merlin microscope (10 kV). The optical images were captured by microscope XZJ-L2030 (Phenix Optics Co.). AFM images were performed by AFM SPI4000 (Seiko Instruments Inc.). The optical transmission spectra were measured by a Hitachi U-3010 spectrometer. Dynamic mechanical analysis (DMA) were taken by DMA Q800 (TA Instruments) scanning from room temperature to 70 °C, with a ramping rate of 5 °C  $\text{min}^{-1}$  or scanning from 0.1 to 50 Hz at 37 °C. PLLA- and PLGA-based polymer fibers as well as silica fibers with similar dimensions (diameter:  $\approx 220\,\mu\text{m}$ , length:  $\approx 10\,\text{mm}$ ) were fixed in DMA Q800 and tested. Optical loss coefficients were measured by the cutback technology in the air and water. All the fibers had initial lengths of about 20 mm and were cut by 3 or 4 mm for an individual measurement. The biodegradable fibers were coupled to a 473 nm LED via ceramic ferrules and fiber patches (Fiblaser Tech. Co., Ltd.) and a standard silicon photodiode was used to measure the output power. *In vitro* degradation tests for PLLA fibers and thin films were performed in phosphate buffer solution with pH = 7.4 at 37 °C. To illustrate the light guiding in *in vitro*, fibers were embedded with a hydrogel-based brain phantom made of agarose hydrogel and consisting of agarose (0.5% w/v), hemoglobin (0.2% w/v), and intralipid (1% w/v).<sup>[27]</sup>

**Optical Simulation:** Optical models of biodegradable fibers were established by using Monte-Carlo ray tracing methods (TracePro free trial version).<sup>[28]</sup> Fiber dimensions were as the same as those in experiments, and properties of PLLA (refractive index, loss coefficients, scattering, etc.) were applied.<sup>[12]</sup> Materials with different bulk scattering coefficients (from 1 to 6  $\text{cm}^{-1}$ ) were simulated, with results compared with experiments. The light source for tracing is defined as a random distribution of  $10^5$  rays. Monitors were used to measure the output power at different lengths, from which fiber optical losses were calculated. At the wavelength of 473 nm, the simulated brain tissue in the model has a refractive index of 1.36, a scattering coefficient of 48.0  $\text{mm}^{-1}$ , an anisotropy factor of 0.85, and an absorption coefficient of 0.21  $\text{mm}^{-1}$ .<sup>[13]</sup>

**In Vivo Studies:** Animal care was in accordance with the institutional guidelines of the Tsinghua University. Protocols were proved by the Institutional Animal Care and Use Committee (IACUC) in the Tsinghua University. All animals were socially housed in a 14/10 h (7 a.m.–9 p.m.) light/dark cycle, with food and water *ad libitum*. The Camkii-Cre (007612) mice were distributed from Jackson Laboratories. C57BL/6 wild-type mice were obtained from Beijing Vital River Laboratory Animal Technology Co., Ltd.

**Biocompatibility Evaluation:** In biocompatibility evaluation, PLGA 50:50 fibers were implanted to a depth of 2.5 mm into the hippocampus of mice (anteroposterior/AP,  $-1.5\,\text{mm}$ ; mediolateral/ML,  $\pm 2.0\,\text{mm}$ ; dorsoventral/DV,  $-2.5\,\text{mm}$ ). The horizontal section and immunostaining were performed (see details in subsection “Immunohistochemistry” in the Experimental Section).

**Immunohistochemistry:** Mice were overdosed with phenobarbital sodium (400  $\mu\text{L}$ , 2% w/v) and perfused transcardially with cold PBS, followed by paraformaldehyde (PFA, 4%) in PBS. Brains were extracted from the skulls and kept in PFA (4%) at 4 °C overnight, then transferred to sucrose (20%) in PBS. 50  $\mu\text{m}$  coronal slices were taken using a vibratome and collected in cold PBS. For DAPI staining, each slice was placed DAPI in PBS (1:10 000 dilution) for 40 min at 37 °C, and for NeuN staining, Chk pAB to FOX3/NeuN antibody (ab134014, Lot GRp0717-3) was first used incubated at 4 °C overnight and then, Alexa Fluor 568 goat anti-chicken IgG(H+L) antibody was used incubated at 37 °C for 40 min. Slices had then undergone three steps for 5 min each in PBS, followed by adding some Antifade Mounting Medium (P0126, Beyotime) and covering slipping on microscope slides.

**Stereotaxic Virus Injection:** All mice were about three months old when they received virus injection. Mice were kept anesthetized using isoflurane (2.0% v/v). Mice were immobilized in custom-built stage-mounted ear bars and a nosepiece. All mice were injected bilaterally with AAV-CMV-EGFP (0.5  $\mu\text{L}$ ) for the injection of HY (in fluorescence recording experiments) or AAV-EF1a-DIO-oCHIEF-mCherry virus (2  $\mu\text{L}$ ) for the injection of HPC (in optogenetic stimulation experiments) (titer  $5 \times 10^{12}$  TU  $\text{mL}^{-1}$ , purchased from Neuron Biotech Co. Ltd.). Injection speed was at a rate of 0.1  $\mu\text{L min}^{-1}$ . The coordinates used were  $-2.0\,\text{mm AP}$ ,  $-1.5\,\text{mm ML}$ ,  $-1.5\,\text{mm DV}$  for hippocampus injections, and  $-2.0\,\text{mm AP}$ ,  $-1.5\,\text{mm ML}$ ,  $-5.5\,\text{mm DV}$  for hypothalamus injections. The needle was slowly lowered to the target site and remained for 3 min before the injection. The needle was also kept at the target site for another 3 min postinjection before slowly withdrawn. All mice were allowed to recover in a home cage for two weeks before all subsequent experiments.

**Fluorescence Photometry:** For the mice used for fluorescence photometry to record EGFP signals in HY, EGFP express was introduced by AAV-CMV-EGFP (0.5  $\mu\text{L}$ ) (see details in subsection “Stereotaxic Virus Injection” in the Experimental Section). PLLA fibers and/or silica fibers with the same lengths (5.5 mm) were ended above the injection site of HY (AP,  $-2.0\,\text{mm}$ ; ML,  $-1.5\,\text{mm}$ ; DV,  $-5.5\,\text{mm}$  from skull). A layer of adhesive cement was applied followed with dental cement to secure the optical fiber implant. Mice were put on a heating pad until fully recovered from anesthesia. All fiber placements and viral injection sites were histologically verified post experiments. As criteria, mice with virus expression mainly in HY were only included. The fiber-based fluorescence photometry system was bought from Thinker Tech Nanjing Biotech Co., Ltd. Excitation light (220  $\mu\text{W}$ ) from a 488 nm semiconductor laser was coupled to implanted PLLA or silica fibers. Emitted green fluorescence signals were collected with the same fibers and then detected by a photomultiplier tube after filtering by a GFP bandpass emission filter. Signals were recorded at a sampling frequency of 100 Hz by an automated data acquisition system (Thinker Tech Nanjing Biotech Co., Ltd.), and further analyzed in Matlab.

**Optogenetic Stimulation:** PLLA and silica fibers were implanted after two weeks of virus injection of AAV-EF1a-DIO-oCHIEF-mCherry (2  $\mu\text{L}$ ) in HPC (see details in subsection “Stereotaxic Virus Injection” in the Experimental Section). During the experiments, mice had undergone a 2 min habituation of the large arena (TSE Systems, Inc.) followed by a 2 min (light off)–2 min (light on)–2 min (light off)–2 min (light on) stimulation procedure. The input laser power (488 nm) was fixed at 13 mW to maintain a mild stimulation. Built-in programs (TSE Systems, Inc.) were used to quantify the travelling distance and the locomotion velocity of mice.

## Supporting Information

Supporting Information is available from the Wiley Online Library or from the author.



## Acknowledgements

R.F., W.L., and R.N. contributed equally to this work. R.F., D.T., and K.Z. acknowledge the support from the Tsinghua Student Research Training (SRT) Program. R.N. acknowledges the support from the China Scholarship Council (CSC). L.Y. and X.S. acknowledge the support from the National Natural Science Foundation of China (NSFC Projects 51602172 and 51601103) and the 1000 Youth Talents Program in China. The authors thank W. Zhang (Tsinghua University) for valuable discussions.

## Conflict of Interest

The authors declare no conflict of interest.

## Keywords

biodegradable devices, fluorescence detection, implantable devices, optical fibers, optogenetics

Received: September 3, 2017

Revised: October 18, 2017

Published online: December 21, 2017

- [1] a) K. Deisseroth, *Nat. Methods* **2011**, *8*, 26; b) M. R. Warden, J. A. Cardin, K. Deisseroth, *Annu. Rev. Biomed. Eng.* **2014**, *16*, 103.
- [2] L. A. Gunaydin, L. Groseknick, J. C. Finkelstein, I. V. Kauvar, L. E. Fenno, A. Adhikari, S. Lammel, J. J. Mirzabekov, R. D. Airan, K. A. Zalocusky, K. M. Tye, P. Anikeeva, R. C. Malenka, K. Deisseroth, *Cell* **2014**, *157*, 1535.
- [3] S. H. Yun, S. J. Kwok, *Nat. Biomed. Eng.* **2017**, *1*, 0008.
- [4] a) A. Sridharan, S. D. Rajan, J. Muthuswamy, *J. Neural Eng.* **2013**, *10*, 066001; b) L. Groseknick, J. H. Marshel, K. Deisseroth, *Neuron* **2015**, *86*, 106; c) A. Gilletti, J. Muthuswamy, *J. Neural Eng.* **2006**, *3*, 189.
- [5] a) A. Canales, X. Jia, U. P. Froriep, R. A. Koppes, C. M. Tringides, J. Selvidge, C. Lu, C. Hou, L. Wei, Y. Fink, P. Anikeeva, *Nat. Biotechnol.* **2015**, *33*, 277; b) S. Park, Y. Guo, X. Jia, H. K. Choe, B. Grena, J. Kang, J. Park, C. Lu, A. Canales, R. Chen, Y. S. Yim, G. B. Choi, Y. Fink, P. Anikeeva, *Nat. Neurosci.* **2017**, *20*, 612.
- [6] a) P. Gentile, V. Chiono, I. Carmagnola, P. V. Hatton, *Int. J. Mol. Sci.* **2014**, *15*, 3640; b) M. S. Lopes, A. L. Jardini, R. M. Filho, *Procedia Eng.* **2012**, *42*, 1402.
- [7] a) S. Hwang, H. Tao, D. Kim, H. Cheng, J. Song, E. Rill, M. A. Brenckle, B. Panilaitis, S. M. Won, Y. Kim, Y. Song, K. Yu, A. Ameen, R. Li, Y. Su, M. Yang, D. L. Kaplan, M. R. Zakin, M. J. Slepian, Y. Huang, F. G. Omenetto, J. A. Rogers, *Science* **2012**, *337*, 1640; b) S. K. Kang, R. K. Murphy, S. W. Hwang, S. M. Lee, D. V. Harburg, N. A. Krueger, J. Shin, P. Gamble, H. Cheng, S. Yu, Z. Liu, J. G. McCall, M. Stephen, H. Ying, J. Kim, G. Park, R. C. Webb, C. H. Lee, S. Chung, D. S. Wie, A. D. Gujar, B. Vemulapalli, A. H. Kim, K. M. Lee, J. Cheng, Y. Huang, S. H. Lee, P. V. Braun, W. Z. Ray, J. A. Rogers, *Nature* **2016**, *530*, 71.
- [8] E. Ceci-Ginistrelli, D. Pugliese, N. G. Boetti, G. Novajra, A. Ambrosone, J. Lousteau, C. Vitale-Brovarone, S. Abrate, D. Milanese, *Opt. Mater. Express* **2016**, *6*, 2040.
- [9] S. Nizamoglu, M. C. Gather, M. Humar, M. Choi, S. Kim, K. S. Kim, S. K. Hahn, G. Scarcelli, M. Randolph, R. W. Redmond, S. H. Yun, *Nat. Commun.* **2016**, *7*, 10374.
- [10] a) M. Choi, J. W. Choi, S. Kim, S. Nizamoglu, S. K. Hahn, S. H. Yun, *Nat. Photonics* **2013**, *7*, 987; b) M. Choi, M. Humar, S. Kim, S. H. Yun, *Adv. Mater.* **2015**, *27*, 4081; c) J. Guo, X. Liu, N. Jiang, A. K. Yetisen, H. Yuk, C. Yang, A. Khademhosseini, X. Zhao, S. H. Yun, *Adv. Mater.* **2016**, *28*, 10244; d) A. K. Yetisen, N. Jiang, A. Fallahi, Y. Montelongo, G. U. Ruiz-Esparza, A. Tamayol, Y. S. Zhang, I. Mahmood, S. A. Yang, K. S. Kim, H. Butt, A. Khademhosseini, S. H. Yun, *Adv. Mater.* **2017**, *29*, 1606380.
- [11] a) S. T. Parker, P. Domachuk, J. Amsden, J. Bressner, J. A. Lewis, D. L. Kaplan, F. G. Omenetto, *Adv. Mater.* **2009**, *21*, 2411; b) H. Tao, J. M. Kainerstorfer, S. M. Siebert, E. M. Pritchard, A. Sassaroli, B. J. Panilaitis, M. A. Brenckle, J. J. Amsden, J. Levitt, S. Fantini, *Proc. Natl. Acad. Sci. USA* **2012**, *109*, 19584.
- [12] a) M. H. Hutchinson, J. R. Dorgan, D. M. Knauss, S. B. Hait, *J. Polym. Environ.* **2006**, *14*, 119; b) R. Auras, B. Harte, S. Selke, *Macromol. Biosci.* **2004**, *4*, 835.
- [13] S. L. Jacques, *Phys. Med. Biol.* **2013**, *58*, 5007.
- [14] J. Sun, S. J. Lee, L. Wu, M. Sarntinoranont, H. Xie, *Opt. Express* **2012**, *20*, 1084.
- [15] C. Marega, A. Marigo, V. Di Noto, R. Zannetti, A. Martorana, G. Paganetto, *Macromol. Chem. Phys.* **1992**, *193*, 1599.
- [16] Y. Wang, B. Steinhoff, C. Brinkmann, I. Alig, *Polymer* **2008**, *49*, 1257.
- [17] S. Lyu, D. Untereker, *Int. J. Mol. Sci.* **2009**, *10*, 4033.
- [18] a) M. Gonzalez, R. Ruseckaite, T. Cuadrado, *J. Appl. Polym. Sci.* **1999**, *71*, 1223; b) V. Piemonte, *J. Polym. Environ.* **2013**, *21*, 313.
- [19] M. G. Kuzyk, *Polymer Fiber Optics: Materials, Physics, and Applications*, CRC Press, Boca Raton, FL, USA **2006**.
- [20] a) M. Pekny, M. Nilsson, *Glia* **2005**, *50*, 427; b) S. Robel, B. Berninger, M. Götz, *Nat. Rev. Neurosci.* **2011**, *12*, 88; c) M. V. Sofroniew, H. V. Vinters, *Acta Neuropathol.* **2011**, *119*, 7.
- [21] E. Papadakis, S. Nicklin, A. Baker, S. White, *Curr. Gene Ther.* **2014**, *4*, 89.
- [22] a) R. J. Racine, *Electroencephalogr. Clin. Neurophysiol.* **1972**, *32*, 281; b) G. M. Alexander, S. C. Rogan, A. I. Abbas, B. N. Armbruster, Y. Pei, J. A. Allen, R. J. Nonneman, J. Hartmann, S. S. Moy, M. A. Nicoletis, J. O. McNamara, B. L. Roth, *Neuron* **2009**, *63*, 27.
- [23] J. Y. Lin, M. Z. Lin, P. Steinbach, R. Y. Tsien, *Biophys. J.* **2009**, *96*, 1803.
- [24] L. T. Lim, R. Auras, M. Rubino, *Prog. Polym. Sci.* **2008**, *33*, 820.
- [25] a) H. L. Hernandez, S. K. Kang, O. P. Lee, S. W. Hwang, J. A. Kaitz, B. Inci, C. W. Park, S. Chung, N. R. Sottos, J. S. Moore, J. A. Rogers, S. R. White, *Adv. Mater.* **2014**, *26*, 7637; b) C. W. Park, S. K. Kang, H. L. Hernandez, J. A. Kaitz, D. S. Wie, J. Shin, O. P. Lee, N. R. Sottos, J. S. Moore, J. A. Rogers, S. R. White, *Adv. Mater.* **2015**, *27*, 3783.
- [26] C. Lu, S. Park, T. J. Richner, A. Derry, I. Brown, C. Hou, S. Rao, J. Kang, C. T. Mortiz, Y. Fink, P. Anikeeva, *Sci. Adv.* **2017**, *3*, e1600955.
- [27] a) P. Lai, X. Xu, L. V. Wang, *J. Biomed. Opt.* **2014**, *19*, 035002; b) E. L. Madsen, M. A. Hobson, H. Shi, T. Varghese, G. R. Frank, *Phys. Med. Biol.* **2005**, *50*, 5597.
- [28] Lambda Research Corporation, <https://www.lambdaresearch.com/trials/> (accessed: June 2017).